


## Article

# GIS-Based Digital Twin Model for Solar Radiation Mapping to Support Sustainable Urban Agriculture Design

Matteo Clementi <sup>1,\*</sup>, Valentina Dessì <sup>1</sup>, Giulio Maria Podestà <sup>2</sup>, Szu-Cheng Chien <sup>3</sup>, Barbara Ang Ting Wei <sup>3</sup> and Elena Lucchi <sup>1,4</sup>

<sup>1</sup> Department of Architecture and Urban Studies (DAStU), Politecnico di Milano, 20133 Milan, Italy; valentina.dessi@polimi.it (V.D.); elena.lucchi@polimi.it or elena.lucchi@unipv.it (E.L.)

<sup>2</sup> Nitter Betanit, 29121 Piacenza, Italy; gpodesta@betanit.com

<sup>3</sup> Engineering Cluster, Singapore Institute of Technology, Singapore 138683, Singapore; szucheng.chien@singaporetech.edu.sg (S.-C.C.); barbara.ang@singaporetech.edu.sg (B.A.T.W.)

<sup>4</sup> Dipartimento di Ingegneria Civile e Architettura (DICAr), University of Pavia, 27100 Pavia, Italy

\* Correspondence: matteo.clementi@polimi.it

**Abstract:** The integration of urban agriculture into cityscapes necessitates a comprehensive understanding of multiple engineering and environmental factors, including urban fabric, building configurations, and dynamic energy and material flows. In contrast to rural settings, urban areas introduce complexities such as hygrothermal fluctuations, variable sunlight exposure and shadow patterns, diverse plant dimensions and shapes, and material interception. To address these challenges, this study presents an open-source Digital Twin model based on the use of a geographical information system (GIS) for near-real-time solar radiation mapping. This methodology aims to optimize crop productivity, enhance resilience, and promote environmental sustainability within urban areas and enables the near-time mapping of the salient features of different portions of the city using available open data. The work is structured into two main parts: (i) definition of the GIS-based Digital Twin model for mapping microclimatic variables (in particular solar radiation) to support sustainable urban agriculture design and (ii) application of the model to the city of Milan to verify its replicability and effectiveness. The key findings are connected to the possibility to integrate open data (solar radiation) with measurements in situ (illuminance and data referred to the specific crops, with related conversion coefficient) to develop a set of maps helpful for urban farmers but also for designers dealing with the synergy between buildings and urban farms. Initially tested on a neighborhood of Milan (Italy), the model will be applied in the Singapore context to verify analogies and differences. This correlation facilitates a more practical and straightforward examination of the relationships between solar irradiation and illuminance values of natural sunlight (involving both incident and diffuse light). The consistency of measurements allows for the precise documentation of these fluctuations, thereby enhancing the understanding of the influence of solar radiation on perceived luminance levels, particularly in urban environments characterized by diverse contextual factors such as vegetation, nearby structures, and geographical positioning.

**Keywords:** building-integrated agriculture; solar maps; photosynthetically active radiation (PAR); daily light integral (DLI); geographic information system (GIS)



**Citation:** Clementi, M.; Dessì, V.; Podestà, G.M.; Chien, S.-C.; Wei, B.A.T.; Lucchi, E. GIS-Based Digital Twin Model for Solar Radiation Mapping to Support Sustainable Urban Agriculture Design. *Sustainability* **2024**, *16*, 6590. <https://doi.org/10.3390/su16156590>

Academic Editor: Jianming Cai

Received: 30 May 2024

Revised: 26 July 2024

Accepted: 30 July 2024

Published: 1 August 2024



**Copyright:** © 2024 by the authors. Licensee MDPI, Basel, Switzerland. This article is an open access article distributed under the terms and conditions of the Creative Commons Attribution (CC BY) license (<https://creativecommons.org/licenses/by/4.0/>).

## 1. Introduction

In recent years, cities have experienced increasingly intense heat waves, excessive rainfall events, and longer periods of drought, posing significant risks to urban infrastructure, public health, and overall livability. The implementation of adaptation and mitigation strategies is crucial for reducing the impact of climate change [1]. Urban agriculture (UA) provides numerous environmental, social, and economic benefits in this direction [2], including climatic resilience, heat island mitigation, runoff management, local food production, environmental quality improvement, biodiversity protection, community inclusion,

job creation, poverty reduction, circular economy, health, and social justice [3,4]. A central theme concerns the reduction in pressure on rural agriculture to ensure a sustainable food supply, strengthen local food systems, and reduce emissions associated with their transport [5]. One important benefit is the cultivation of a diverse range of crops [2] while occupying minimal urban space [6]. Beyond their localized impact, ground-based UA faces challenges from urban sprawl contributing to the global ecological balance, urban resilience, and biodiversity conservation [7]. The integration of green spaces in urban areas offers not only ecological benefits but also significant social advantages [8]. Apart from their aesthetic appeal, these spaces facilitate a sense of community [5], offering areas for social cohesion, community networks, education, learning, knowledge exchange, and engagement in recreational activities, social interactions, and connectivity [9]. Conversely, UA applications are limited by inherent drawbacks that include health security, scarcity of urban land caused by ongoing city expansions, high initial costs, need for specialized knowledge and skills, and accurate urban space planning [9]. Other concerns regard the extensive use of water for irrigation, contamination by pathogens due to inappropriate use of organic fertilizer, presence of insects and other small animals near inhabited areas, energy-intensive infrastructure, and high energy demands associated with space conditioning systems [4]. Careful selection of the site, urban agriculture techniques, and plant characteristics is essential to avoid environmental issues [10]. Thus, the definition of robust policies that address all the complex issues related to urban development lack of space, economic inequalities, food justice, and public health is essential to promote the diffusion of UA strategies [5]. These policies need to be adaptable and responsive to changing needs and innovative technological developments for integrating agricultural systems into cities (e.g., vertical farming, green rooftops, hydroponics, and aquaponics) [2]. Thus, for policy-makers, it is crucial to adopt evidence-based policies based on an accurate assessment of environmental resource availability [10].

However, UA implementation depends on a complex interplay of climatic conditions, seasonal variations, agricultural practices, and social dynamics within urban settings [11]. Therefore, a comprehensive understanding of the physical capacity, availability, and suitability of urban built and open spaces is essential to identify areas that would benefit from UA [12]. In contrast to rural settings, urban environments introduce additional complexities that must be carefully considered to optimize the coexistence of plants and anthropic activities for food production. Thus, integrating UA into urban environments necessitates a comprehensive understanding of several factors, such as urban fabric, building configurations, and dynamic energy and material flows. These complexities include hygrothermal fluctuations, sunlight exposure, shadow patterns, plant dimensions and shape, material interception, etc. To this purpose, the urban metabolism approach [13] delineates the dynamic flow of materials, energy, and resources within urban ecosystems, drawing parallels with how organisms in natural ecosystems utilize resources such as water, nutrients, and microclimate [14]. This analysis is supported by open digital documentation on the physical and morphological characteristics of the city, buildings, soils, and subsoils as well as the presence of vegetation, water, and microclimatic data. The integration of different datasets enables their use as inputs for UA implementation considering thermal behaviors of buildings, water requirements for plants or local inhabitants, and environmental factors for plants' growth (e.g., sunlight exposure, shadows, solar radiation, daylight, air temperature, wind speed, relative humidity, etc.).

Geographical information system (GIS) tools play a crucial role in mapping the urban metabolism for defining UA production areas that balance physical and socio-economic factors [15]. GIS applications in urban agriculture allow for the detailed analysis of spatial data to assess the suitability of different urban sites for agricultural use. GIS mapping methodologies have been particularly developed in the agricultural sector to define the distribution of water and nutrients, which is a central concern for researchers, industries, and farmers. Water mapping generates accurate visual representations of water distribution within the soil, facilitating the identification of irrigation needs and areas vulnerable to flooding or

waterlogging to optimize water resource management [16]. Similarly, nutrient mapping allows for the evaluation of nutrient availability and distribution, which is essential for optimizing plant growth, yield, and crop quality while also reducing the environmental impact of excessive fertilizer use [17]. Although previous studies have highlighted the importance of microclimate mapping in reducing the heat island [18] and improving green design [19,20], there is a lack of research specifically focused on the development of GIS-based approaches for solar radiation mapping across urban areas, which is essential for optimizing the placement and design of UA installations [21]. Various methodologies, also supported by GIS tools, are available to estimate solar irradiance in a city for installing photovoltaic and solar thermal systems [22,23]. Conversely, there are none specifically dedicated to UA installation [24] despite their potential to support the UA design and management for the ensuring necessary light for plants to grow in a healthy and productive manner [25]. Solar radiation mapping methodologies help estimate solar irradiance [ $W/m^2$ ], photosynthetically active radiation (PAR) [19], and the daily light integral (DLI), which are vital for plant health and productivity [21]. Solar irradiance represents the power of solar energy received per unit area [18]; PAR is the spectrum range of solar radiation absorbable by chlorophyll, which activates the process of converting carbon dioxide and water into glucose and oxygen [19]; and DLI represents the total amount of PAR received by a plant over the course of a day [20]. The integration of these solar mapping techniques with GIS allows for precise identification of areas with sufficient sunlight, ensuring optimal growth conditions for various crops.

The concept of a Digital Twin has increasingly been applied to agricultural landscapes for monitoring and optimizing agricultural systems, with a particular focus on vertical farming and urban agriculture. Digital Twins offer a sophisticated approach by providing a digital replica of physical assets, systems, or processes in urban environments. This technology enables continuous monitoring and real-time data analysis, which is crucial for the adaptive management of UA installations [26]. Naval et al. [27] utilized Digital Twins to validate irradiance, temperature, and humidity across various buildings. These parameters were incorporated into building energy simulations to generate potential maps for growing different vegetable species. Their results revealed that both rooftops and building facades present significant opportunities for vertical vegetable cultivation. Ghandar et al. [28] proposed a cyber–physical implementation of aquaponics enhanced with adaptive capabilities through a Digital Twin system and machine learning. Their study demonstrated how the integration of real-time data, predictive modeling, and decision analytics can effectively enhance data-driven decision making in aquaponic system production. Mengi et al. [29] introduced a framework that combines Digital Twins with rapid optimization techniques for the optical design of indoor farming systems. Their focus was on optimizing the distribution of lighting systems to maximize plant growth and energy efficiency. By simulating various lighting conditions and configurations, their model facilitated rapid testing and refinement of the optical setup. Lastly, Gabriele et al. [30] integrated Earth Observation data with local information to monitor climate change and assess human impacts on heritage buildings and protected landscapes. They combined environmental-scale analysis, utilizing historical maps and the normalized difference vegetation index, with local-scale multi-sensor surveys that extract 3D vegetation models. This approach helped establish conservation criteria for the sustainable management of biodiversity.

The integration of Digital Twins with GIS mapping can further enhance the accuracy and applicability of these analyses by creating dynamic models that reflect real-time conditions and simulate different scenarios for UA development [25]. They allow the management of extensive information for systematic analysis and scenario definition, prompting the integration of GIS maps with Digital Twin as a suitable decision-support tool for UA design objects [26]. Their integrated application opens new research possibilities in urban planning and policy making. For instance, Digital Twins can simulate the impact of varying solar radiation levels on crop growth, allowing for proactive adjustments in agricultural practices to optimize yields and resource use. Additionally, this integration

supports scenario-based planning, where policymakers can evaluate the effects of different urban development strategies on UA feasibility and productivity. Despite this, the literature review revealed a lack of studies on GIS-based Digital Twin models in the context of UA.

Considering the intricate interplay between UA and metabolism mapping using GIS tools and Digital Twins data, current gaps in the literature refer to the following:

- Absence of specific microclimatic mapping methodologies to support UA design, installation, and management based on dynamic climate factors crucial for plant growth, food productivity, and sustainable agricultural practices;
- Lack of GIS-based methodologies for accurately estimating solar irradiance to design and manage UA practices, considering spatial and temporal variations in sunlight availability;
- Lack of research on the practical application of Digital Twins for modelling and simulating solar irradiation dynamics in UA systems practices;
- Need for integration of environmental parameters, GIS, and Digital Twins to maximize the efficiency and sustainability of planning, design, and management of UA initiatives.

To address these gaps, the present study aims to develop and validate a GIS-based Digital Twin model that integrates critical microclimatic variables essential to support the planning, design, and management of sustainable UA initiatives within urban environments. By addressing current gaps in the literature, this study's aims are as follows:

- Develop a specific microclimatic mapping methodology to enhance UA design, installation, and management, focusing on dynamic solar radiation factors crucial for plant growth, food productivity, and sustainable agricultural practices;
- Establish GIS-based methodologies for accurately estimating solar irradiance, considering spatial and temporal variations in sunlight availability, to optimize UA practices;
- Integrate environmental parameters, GIS, and Digital Twins to maximize the efficiency and sustainability of UA planning, design, and management.

This model uses open-source tools and databases to continuously record urban features and perform real-time mapping, enhancing cost effectiveness, customization, and data integration. The integration of GIS maps with Digital Twins offers a decision-support tool for UA. Digital Twins can provide a comprehensive and dynamic overview of urban environments, incorporating real-time data and simulations to optimize the placement and management of UA systems. This technology enables continuous monitoring and adaptive management, ensuring that UA installations can respond effectively to changing environmental conditions and urban development patterns. Thus, the ultimate goal is to empower informed decision making and collaborative efforts in urban planning and management that are essential for evaluating current conditions and designing future scenarios, particularly in adopting advanced food technologies.

## 2. Methodology

The proposed model is part of the “*Building-Integrated Zero Emission Urban Farming*” (Bize\_UrFarm) research initiative. This project involves collaboration between the Politecnico di Milano, the Singapore Institute of Technology (SIT), and other technical partners, partially funded by the Italian Ministry of Foreign Affairs and International Cooperation (MAECI) through a bilateral agreement between Italy and Singapore. The two research groups encompass a diverse array of expertise, ranging from architecture (with specialists in urban metabolism, climate change adaptation and thermal comfort, and natural and artificial lighting) to materials chemistry and agronomy. This interdisciplinary integration creates a compelling synergy for developing zero-emission-integrated architectural systems, as outlined in the research program, and for providing design guidelines to public administrations and private entities.

Additionally, the project involves not only representatives from the academic world but also firms interested in advancing knowledge derived from the integration of light-

ing and agricultural production. This includes companies engaged in the urban/vertical farming sector, who are willing to collaborate in the development of innovative building envelopes. The initiative adopts a cross-disciplinary approach, addressing different issues related to local food production, self-sufficiency, environmental and energy-efficient building renovations, social inclusion, biodiversity preservation, and the continuity of green corridors within urban landscapes to mitigate climate impacts.

This iterative process aims to validate and enhance the proposed model. The study reported in the research is structured into two main sections:

- Definition of the GIS-based Digital Twin model for mapping microclimatic variables (in particular solar radiation) to support sustainable UA design (Section 3);
- Application of the model to the Italian case study (Section 4).

The first section (Section 3) focuses on the definition of a GIS-based Digital Twin model designed to map microclimatic variables, particularly hygrothermal, solar radiation, and natural light parameters, to provide detailed and accurate data on microclimatic conditions crucial for a dynamic optimization of UA design and management.

The second section (Section 4) involves the practical application of this model to a case study at the border between the urban and rural environment in the city of Milan (Italy). By applying the model to a real-world scenario, the research seeks to validate its effectiveness and demonstrate its utility in guiding UA initiatives. This application highlights how the model can be used to make informed decisions about UA design, considering local microclimatic conditions and the specific needs of the urban environment.

### 3. Definition of the GIS-Based Digital Twin Model

The GIS-based Digital Twin Model for microclimatic variables mapping is based on the use of open-source tools and data [31]. Different open-source GIS are available, such as Quantum GIS (QGIS) [32], Geographic Resources Analysis Support System (GRASS-GIS) [33], gvSIG [34], etc. These tools offer interoperability, allowing different systems to work together seamlessly, and customizability, enabling users to tailor the software to their specific needs. Additionally, they facilitate the integration of diverse datasets and plugins, enhancing their functionality and versatility in handling geographical data. Nevertheless, the single software may suffer from a lack of some advanced features compared to commercial alternatives, but the open-source nature of the software means that their implementation is oriented towards mutual integration rather than competition. The lack of advanced features for specific analysis of a software is compensated by the interoperability among them and by the free access that allows the use of groups of programs on the same platform rather than just one, allowing use of GIS, which has broader functionality, such as through QGIS [32], and with software that has advanced features such as GRASS-GIS [33]. Choosing a suitable group of open-source GIS tools is consequently important. In the specific case of this paper, the software used were QGIS and GRASS-GIS [33]. QGIS [32] has been considered the most appropriate for its comprehensive suite of tools and functionalities, extensive customization, and wide range of plug-ins and extensions for spatial analysis, data visualization, and map creation. GRASS-GIS [33] has been used for advanced processing related to solar radiation mapping [35]. In both cases, the availability of multiple operating systems (e.g., Windows, macOS, and Linux) and data formats (e.g., Esri Shapefile, GeoTIFF, and File Geodatabase) also ensures compatibility with diverse computing environments. This level of compatibility is crucial for multidisciplinary projects and is more versatile compared to some other GIS tools. Furthermore, QGIS is open-source and free to use, making it accessible for a broader range of users, including those with limited budgets. It benefits from a community-driven approach that encourages collaboration, feedback, and continuous improvement, ensuring regular updates and improvements. This community-driven approach fosters collaboration and feedback, which can be less pronounced in proprietary software. The limitations found in the integrated use of the two software are linked to the different methods of use and interface. QGIS presents a mode of use similar to proprietary software and is easier to understand, while GRASS-GIS presents

more unique and specific features and requires dedicated training activities for its use. At the current stage of software development, some GRASS-GIS features have been integrated into QGIS, but some processing is possible only through the direct use of GRASS-GIS, as in the specific case of solar radiation mapping.

Moreover, to delve into the social aspects, a dataset of specific information is requested to be mapped to facilitate the correlation with socio-economic needs and the identification of intervention priorities. Some key indicators are mapped on the “*demographic area units*” or “*demographic data collection units*”, such as the census blocks (CBs), the output areas (OA), or the census output areas (COA). Generally, these units contain demographic, economic, and housing information. Thus, this method enables the integration of demographic data with other variables, also maximizing the accuracy and detail of the mapping. This choice promotes the method’s replicability because these units are standardized and defined by the census. Therefore, the data collected on these units are consistent and comparable across different geographical areas and over time. Furthermore, the association between these units and the Digital Twin facilitated the identification and use of the various social dynamics mapped within the urban environment, thereby supporting the selection of tailored UA interventions.

The microclimatic variables affecting urban agricultural production include the following:

- Air temperature and relative humidity mapping;
- Solar radiation and natural light mapping.

Understanding the spatial and temporal distribution of air temperature ( $T_a$ ), relative humidity ( $RH_a$ ), solar radiation, and natural light distribution is crucial for optimizing crop growth and mitigating potential risks associated with environmental stressors. Additionally, these parameters are important for preventing or managing pest infestations and plant diseases, contributing to plant health with targeted pest control measures, and for irrigation schedules.

The development of a GIS-based Digital Twin model for mapping microclimate variables requires the integration of representative mean and real-time data. The mean data can be based on the typical meteorological year (TMY), which is a set of meteorological data derived from historical weather observations. These data are statistically processed to create a representative dataset of typical weather conditions for a specific location and period. The real-time data collection is based on various climate monitoring units in urban and peri-urban areas that publicly release their data (e.g., [36]). This approach enriches the published information on typical meteorological data by incorporating significant real-time updates, thereby increasing accessibility through a unified GIS platform.

In the first case, the mean values for  $T_a$  and  $RH_a$  can be extracted from open-source datasets, such as the PVGIS TMY generator [37]. Unfortunately, these mean values cannot fully capture localized variations in microclimates, which are influenced by factors such as topography, soil composition, and canopy cover. Therefore, significant deviations from the actual environmental conditions can occur. Consequently, the map does not accurately reflect the localized variations of  $T_a$  and  $RH_a$ , producing a constant and homogeneous distribution value. Instead of relying solely on mean values, integrated approaches should combine remote sensing technologies such as satellites, drones, and sensor networks equipped with Internet of Things (IoT) devices. Indeed, solar mapping can benefit from the use of GIS and Digital Twins tools thanks to the integration of solar irradiance, topography, land cover, and shading effects. The methodology employed to map solar radiation and natural light variables is presented below (Section 3.1).

### 3.1. Solar Radiation and Natural Lighting Mapping

The quantification of solar radiation and natural light on urban surfaces is fundamental for evaluating the energy efficiency of UA systems, especially when integrated in the buildings, such as attached greenhouses on facades or rooftops. The high availability of solar radiation allows the application of strategies for reducing climate-altering emissions in urban areas, allowing the energy useful for UA production to be sourced locally and,

at the same time, promoting bioclimatic strategies for energy saving. On the other hand, the quantification of natural lighting is essential for estimating the luminous comfort of inhabitants and plant well-being according to the photosynthetically active radiation (PAR). Mapping the various characteristics of natural lighting enables the association of production vocations with different parts of the building envelope, thereby identifying the actual agronomic production capacities. Accurate and dynamic mapping of solar radiation, including incident component, natural lighting, and PAR, is necessary to reflect real conditions. The analysis of solar radiation and natural lighting is quite complex due to the interplay between radiation and existing buildings and vegetation, which constitutes a key factor for the assessment of real solar conditions in urban areas. The current development of both open-source and proprietary GIS software allows mapping the influence of obstructions present in urban areas [35]. These calculations consider natural features such as terrain, mountains, hills, and water, excluding buildings and trees. However, precise knowledge of solar radiation components (visible light, ultraviolet, and infrared) is crucial for designing UA systems. In addition, these tools are biased towards analyzing and creating process maps according to the cloud cover, i.e., for clear-skies conditions as well as days with varying radiation conditions, including cloudy and partially cloudy skies. The calculation of PAR maps based on solar radiation data is not a direct process. Rather, it necessitates the conversion of solar radiation into luminous features. This requires an intermediate passage from solar radiation to light levels and finally into PAR values. The procedure used for simulating solar radiation is based on the following phases:

- Creation of a digital elevation model (DEM): a raster map representing the terrain's geometric configuration, associating each pixel with elevation above sea level (Section 3.1.1);
- Solar radiation mapping at different heights to calculate solar radiation data, including direct, diffuse, and reflected radiation (Section 3.1.2);
- PAR and DLI mapping (Section 3.1.3);
- Integration of the Digital Twin with data detected through sensors (Section 3.1.4).

The methodology is described in Figure 1.

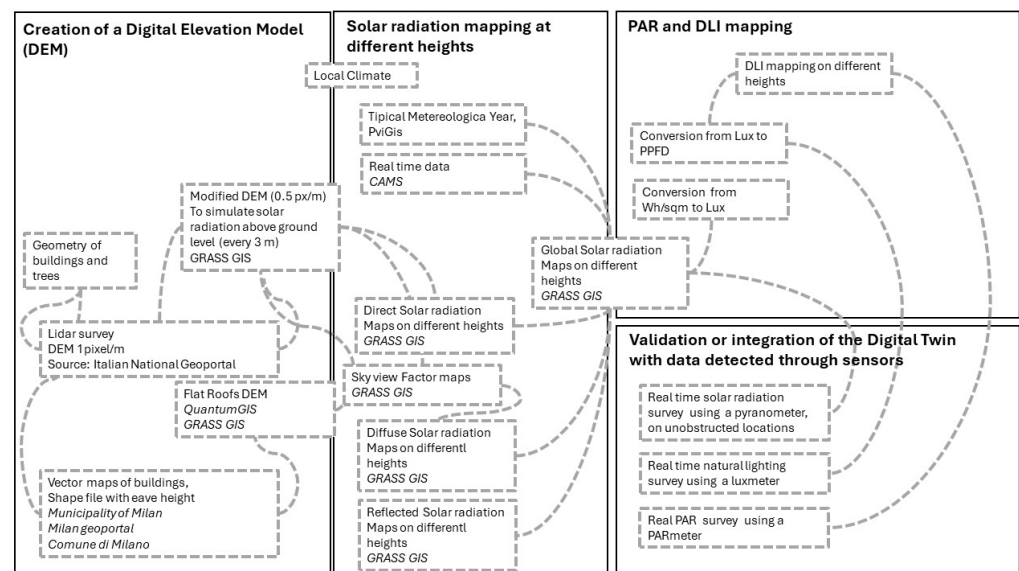


Figure 1. Work methodology (source: Elaboration of the Authors).

### 3.1.1. Creation of a Digital Elevation Model

The first step is to acquire or generate a DEM, which provides detailed information about the topography of the area. A DEM is a raster map where each pixel corresponds to the elevation above sea level of the represented orography. Various techniques can be

employed to create DEMs, depending on factors such as available data, scale, and desired level of detail. These techniques include processing point datasets, vector lines (level curves), or three-dimensional (3D) terrain models. For instance, DEMs can be processed from vector maps, which assign height values to each polygon with respect to ground or sea level, or from light detection and ranging (LIDAR) technology, which uses point cloud data collected from aerial surveys. The DEM resolution varies depending on the size of the area. In urban areas, fine resolutions are required to accurately represent obstructions from buildings. Typically, resolutions, in terms of the number of pixels per dot (DPI), should not exceed one pixel for a surface of  $0.5 \times 0.5$  m or  $1.0 \times 1.0$  m [38]. Higher map resolutions increase the fidelity to the actual site configuration.

### 3.1.2. Solar Radiation Mapping at Different Heights

The second step is the processing of solar maps for each pixel of the DEM, wherein the results are aggregated to form irradiation maps. This process involves computing solar radiation data for each point on the map, including direct, diffuse, and reflected radiation. The calculations can be performed on either the horizontal or inclined plane, depending on the terrain configuration. They can cover specified time intervals ranging from hourly to daily. When assessed in urban areas, with the buildings at different heights, horizontal maps at different heights provide detailed information on the intensity of solar radiation at different levels of the urban space, allowing the assessment of variations in solar exposure. These maps can be used to identify the sunniest and shadiest areas along building facades and to optimize farming irrigation and fertilization based on the specific needs of plants in different areas exposed to the varying amounts of sunlight. Other kinds of maps illustrate the distribution of solar radiation on tilted/vertical building surfaces, highlighting areas of direct sunlight and shadows. These maps can be used to guide the placement of vertical plants to maximize sunlight exposure for each plant, to identify areas of the shadow cast by building elements (e.g., balconies, awnings, or neighboring structures), and to determine areas for shadow-tolerant crops.

The GRASS-GIS open-source GIS package [33] can be utilized to simulate solar radiation on a surface via DEM. This package permits the precise calculations of solar irradiance under various sky conditions, including clear-skies and cloud-cover conditions. The “slop-aspect” command facilitates this process by associating orientation and slope degrees with each pixel of the DEM. To calculate the irradiance in  $\text{Wh}/\text{m}^2$  under clear skies, Linke turbidity and albedo coefficients can be used to set the maps. The Linke turbidity coefficient quantifies the atmospheric turbidity, which affects the scattering and absorption of solar radiation through the atmosphere. This parameter adjusts the amount of diffuse radiation that reaches a specific location, considering atmospheric conditions and their impact on the availability of solar energy. The albedo coefficient represents the ratio of reflected solar radiation to total incident solar radiation on a surface. This parameter assists in accurately representing the reflective properties of surfaces. To create solar maps under clear-sky conditions on specific days and hours, these two maps, in addition to the DEM, should be used. The solar irradiance map under clear-sky conditions is divided into direct and diffuse components on the pixel plane. To have maps at different heights, in GRASS-GIS, all pixels below the desired altitude for the plane are selected, and the altitude value for the plane is specified. Subsequently, the slopes and orientations should be recalculated based on this information, and the maps could be regenerated accordingly. To consider factors such as solar diffusion through atmospheric layers and irradiation conditions under cloudy skies, detailed calculation methods can be employed. These methods are documented in the literature [35].

### 3.1.3. PAR and DLI Mapping

In this step, the critical parameters for plant growth, namely PAR and DLI, are employed to monitor the growth conditions of the plants. PAR refers to solar radiation in the range of wavelengths between 400 and 700 nm, crucial for photosynthesis and plant



growth [39]. The initial layer of photosynthetic cells primarily absorbs red and blue light due to chlorophyll absorbance [40]. The newly introduced measurement quantifies all photons falling within 400–700 nm and is denoted in micromoles per meter per second [ $\mu\text{mol}/\text{m}^2/\text{s}$ ]. Photosynthetic photon flux (PPF) measures the moles of PAR generated by a light source per second [41]. Additionally, photosynthetic photon flux density (PPFD) combines PPF with surface area, expressing the number of PAR photons falling on a specific area in  $\mu\text{mol}/\text{m}^2/\text{s}$  [41]. Analysis of the literature analysis that the conversion factor from lux to PPFD typically ranges from 0.017 to 0.02, with negligible differences. Table 1 below shows the different conversion rates determined by various literatures between the intensity of sunlight in lux to PPFD ( $\mu\text{mol}/\text{m}^2/\text{s}$ ) (Table 1).

**Table 1.** Lux-to-PPFD conversion factor between varying literature reviews (Source: Authors' elaboration).

Author	Lux to PPFD Conversion Factor	City/Country	Climate	Köppen Climate
(Ocampo, 2017) [42]	0.02	Philippines	Tropical rainforest	Af
(Lee and Park, 2013) [43]	0.0185	South Korea	Humid continental	Dwa
(Jarzyna, Podgorska, Szwed, and Jozwiak, 2018) [44]	0.0185	Łysa Góra, SE	Marine west coast	Dfb
(Mazzelli et al., 2019) [45]	0.0185	Rome, Italy	Mediterranean	Csa
(Hall and Rao, 1999) [41]	0.02	London, UK	0.02	London, United
(Ashdown, 2014) [46]	CIE Clear Sky 0.0181 (CIE 5500 K) 0.0183 (CIE 6500 K) 0.0186 (CIE 7500 K) CIE Overcast Sky 0.0178 (CIE 5800 K) 0.0205 (CIE 9300 K)	Victoria, Canada	Warm-summer Mediterranean	Csb
(Fang, Arsano, Brown, Reinhart, and Mueller, 2019) [47]	0.0185	California, USA	Warm-summer Mediterranean	Csb

Asian greens like kailan and nai bai typically thrive with a PPFD between 200 and 300  $\mu\text{mol}/\text{m}^2/\text{s}$ . However, Alahakoon [48] found that increasing PPFD to 500  $\mu\text{mol}/\text{m}^2/\text{s}$  led to a substantial five-fold growth improvement in Asian greens. Moreover, higher PPFD (>300  $\mu\text{mol}/\text{m}^2/\text{s}$ ) resulted in thicker leaves and larger leaf areas [48].

DLI represents the total photosynthetically active photons accumulated per square meter throughout the day. It is expressed as moles of light per square meter per day [ $\text{mol}/\text{m}^2/\text{day}$ ] and depends on light duration and intensity [49]. To calculate DLI, measure PPFD in  $\mu\text{mol}/\text{m}^2/\text{s}$  as it varies during the day. There is a relationship between PPFD and DLI, which is given by the following [50]:

$$\text{DLI} = \text{PPFD} \times \text{light hours per day} \times (3600/1,000,000) \quad (1)$$

DLI significantly impacts plant growth, yield, and quality, including root and shoot development, finishing quality, and timing. Growers can determine when crops need additional lighting or shade by monitoring and recording DLI [49]. The required PPFD and DLI values vary among different crops and plants according to latitudes, climates, etc. The typical DLI ranges from 5 to 25  $\text{mol}/\text{m}^2\cdot\text{day}$ , with an average of 12 to 14  $\text{mol}/\text{m}^2\cdot\text{day}$ . Specific requirements vary for plants. For example, kailan, bok choy, and bayam need very high light levels (47.22, 39.96, and 33.95  $\text{mol}/\text{m}^2\cdot\text{day}$ , respectively), while Chinese cabbage and lettuce thrive under moderate light (19.90, 17.35, and 14.51  $\text{mol}/\text{m}^2\cdot\text{day}$ , respectively) [51]. The Digital Twin model will incorporate data that are collected and specifically tailored to these variations.

The Copernicus Atmosphere Monitoring Service (CAMS) program provides high-quality environmental data and services based on satellite and in situ observations. CAMS data allow for the construction of solar irradiation maps based on actual irradiation conditions. Thus, the creation of maps representing the DLI requires the application of specific conversion coefficients. As mentioned above, the literature data suggest an approximate conversion coefficient from lux to PPFD of 0.02 [48]. To convert solar irradiation maps into DLI maps, an additional step with the corresponding conversion coefficient from Wh/m<sup>2</sup> to PPFD is necessary. According to the method described by Cucumo et al. [52], transforming solar irradiation maps requires multiplication of the values of global solar irradiation incident on a horizontal plane by a conversion factor of 109.54 lm/W to obtain the total lm incident per m<sup>2</sup>, i.e., lux. Then, for an approximate mapping of the DLI using GIS, lux must be converted into PPFD. To this purpose, the result of this calculation must be multiplied by 0.02. Equation (1) permits the calculation of DLI from PPFD. Thus, the total PPFD value should be multiplied by 3600/1,000,000, or 0.0036. Considering that the initial value mapped by the GIS and referring to the global solar radiation on a horizontal surface already accounts for the daily amount, it is not necessary to multiply the data by the number of hours to derive a single conversion coefficient. Consequently, the single coefficient will be the result of the following multiplication:

$$109.54 \times 0.02 \times 0.0036 = 0.00788688 \quad (2)$$

As a result, based on the scientific literature, it is possible to derive a single coefficient to convert the amount of incident solar irradiation into the equivalent DLI.

#### 3.1.4. Integration of the Digital Twin with Data Detected through Sensors

When simulating solar radiation under high sky-cover conditions, specific coefficients and further processing are required (e.g., the cloud-cover index or OKTA). As mentioned before, the first step is the calculation of the irradiation under clear-skies conditions on a horizontal plane and relating to the direct and diffuse component. Then, the reduction coefficient of the direct and diffuse solar irradiation value is calculated based on the representative values of the simulated day. This can be either an average day or a specific day of the year detected through sensors. In this case, both types of processing were used for specific purposes:

- Typical weather data are used for developing maps to support the design and for verifying the effectiveness of specific UA strategies;
- Real-time meteorological data can be used for simulating different variables associated with the solar source, such as natural lighting and PAR, using open-source GIS software.

The TMY data comprise an hourly climatic file that provides not only solar radiation but also other climatic variables such as  $T_a$  and  $RH_a$ . This information is accessible through an online database that allows users to download the TMY dataset for a location identified on the map [53]. This climatic file is used for calculating maps of specific standard days such as the solstices and an equinox.

A second set of maps is based on the real-time solar radiation conditions of a particular day, which were derived from the CAMS calculation model, predominantly focused on the European and North African context [54]. This platform grants access to solar irradiation data recorded at different time intervals (minutes and hours), offering information on real irradiation conditions categorized into diffuse and direct components. Moreover, to have GIS simulations that closely resemble real solar radiation conditions, hourly CAMS data can be used to map hourly solar radiation conditions based on direct and diffuse components. By setting maps based on recorded solar radiation for actual days and accessing data freely, simulated information can be refined using sensor-detected data from the same period. This approach forms the basis for the development of the Digital Twin model to enhance the

real irradiation and natural lighting conditions and verify its effectiveness by comparing the simulated data, using a TMY file, with the actual data.

By correlating data from the CAMS system with lux measurements, coefficients for dynamic luminous efficiency calculations can be derived. This relationship allows for the integration of natural lighting maps with solar radiation maps. Solar radiation, such as global horizontal irradiance (GHI), beam horizontal irradiance (BHI), diffuse horizontal irradiance (DHI), and beam normal irradiance (BNI), and illuminance measured data can be adjusted based on local weather conditions, time of day, and seasonal variations. This is helpful for the calibration of the simulations, leading to more accurate results. This Digital Twin model incorporates diverse datasets that could allow for creating more versatile real-world simulation scenarios towards the optimal urban farming planning and design, while topography, existing infrastructure, and microclimate conditions are also considered. Furthermore, combining maps by integrating illuminance data and solar radiation data leads to more accurate prediction of the incoming solar energy used for photosynthesis and enhanced decision making of sustainable urban farming practices appropriate in the local context [55].

#### 4. Application of the Model to the Italian Case Study

The application is related to the Corvetto neighborhood in the city of Milan (Italy). This neighborhood is situated in the southeastern periphery of Milan, about 4 km from the city center, bordering the urban and rural areas of the Southern Agricultural Park. The area has undergone significant urban and architectural transformations. Initially, it was a small rural town consisting of farmhouses and a neoclassical palace (Villa Gambalavita), which was later converted into a farmstead (Cascina Gamboloita). Due to urbanization, the farmstead was demolished in the early 20th century to make way for the Regina Elena neighborhood (now the Mazzini district). This neighborhood constitutes the first historical nucleus of the area (1925–31). The postwar period saw a significant expansion in the built-up area. This residential complex has a trapezoidal urban structure and includes the Omero (1949), Gabrio Rosa (1948–1951), INA Casa Barzoni and Montemartini (1949–1951), and Barzoni (1952) districts. The construction of an overpass to handle traffic introduced a significant change in the urban morphology (1960). The neighborhood has several functions, including housing, schools, retirement homes, offices, and industries. Residential buildings come in a variety of types, including townhouses, in-line buildings, and arcaded blocks. The Corvetto neighborhood in Milan is currently a transitional area, characterized by a unique mixture of high-density residential buildings and farms. Many of these farms are currently disused or undergoing transformation. There is a lack of green public spaces, causing public activities to be limited to streets and major piazzas. The neighborhood remains a promising location for urban redevelopment and social regeneration (Figure 2).

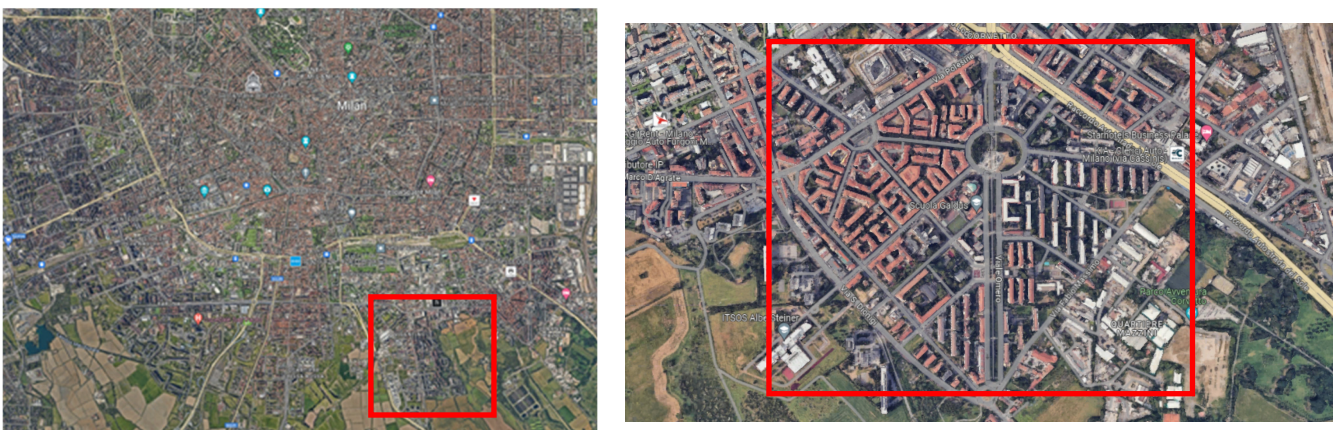


**Figure 2.** Satellite image of the southern part of Milan with the Corvetto neighborhood highlighted in red (source: Elaboration of the Authors from Google Satellite).

The Corvetto neighborhood was mapped using QGIS [32]. Key indicators were mapped based on census blocks (CBs), which represent the smallest geographical units used in Italian open-source data collected during periodic population and housing censuses, which occur typically every 10 years [56]. These CBs contain demographic (e.g., population type and age), economic (e.g., activity and per capita income), and housing (e.g., functions, types, size, and age of buildings) information. The application of the proposed solar radiation mapping methodology to the Corvetto neighborhood is reported below, with the results obtained also shown (Section 4.1).

#### 4.1. Solar Radiation and Natural Lighting Mapping

The initial step in the modelling process for the neighborhood started with the calculation of the DEM, a raster image on a greyscale, through GRASS. In this case, the selected resolution of the model was 0.5 x 0.5 m to obtain high-resolution results. Solar radiation data, including direct, diffuse, and reflected radiation, were calculated for each point of the raster map. The resulting solar radiation maps were raster representations associating each pixel with incident solar radiation over defined time intervals considering the following:

- Creation of a digital elevation model (from LIDAR) (Section 4.1.1);
- Solar radiation mapping at different heights (Section 4.1.2);
- PAR and DLI mapping (Section 4.1.3);
- Integration of the Digital Twin with data detected through sensors (Section 4.1.4).

##### 4.1.1. Creation of a Digital Elevation Model

Solar radiation and natural light were quantified on horizontal planes to consider their impact on most UA installations, such as plants, gardens, rooftops, and vertical farming. Horizontal surfaces were preferred over inclined planes, as they receive maximum solar radiation throughout the day, which aligns with the critical need for sunlight exposure in plant photosynthesis and growth. The calculation of the irradiance for each pixel of the map was carried out starting from the solar constant, which denotes the estimated solar irradiance outside the Earth's atmosphere perpendicular to the sun's rays, with slightly variable values depending on the period of the year and in generally equal to 1367 W/m<sup>2</sup>. For each time interval, solar height and azimuth were determined for each hour of the day within the chosen time interval. Additionally, atmospheric effects and obstructions on the horizon were factored in for each pixel. Hourly solar radiation data, considering direct, diffuse, and reflected components, were accumulated over the desired time frame for simulation. As mentioned before, these values pertain to geometric projections on a horizontal plane of the mapped surfaces characterized by different orientations and inclinations (Figure 3).

##### 4.1.2. Solar Radiation Mapping on the Horizontal Plane at Different Heights

Thus, the solar maps were processed on a fictitious plane parallel to the existing orography at regular height intervals of one meter in height or at the height of the individual floors (3 m) [57]. These calculations illustrate the daily global radiation conditions on a fictitious horizontal plane at different heights from the ground (every 3 m). The processing was conducted on a DEM processed using a LIDAR survey. The availability of the LIDAR survey for the context of Milan facilitated the simulation of obstruction effects caused by buildings and existing vegetation. The same DEM was used to process clipping maps that reveal the satellite images below [58]. Unlike what can be processed from vector maps, a DEM generated from LIDAR allows for consideration of the actual obstruction by vegetation. The clipping masks created at different heights above the ground consider both buildings and trees (Figure 4).

Solar radiation simulations conducted at various heights enable the optimization of plant placement, fostering the creation of microclimates tailored to accommodate a diverse array of plant species with specific light and sun requirements. This approach enhances crop diversity and sustainability in UA. For instance, plants such as spinach, arugula, and

certain varieties of ferns, begonias, and lettuce exhibit adaptability to lower levels of solar irradiance, around  $200 \text{ Wh/m}^2$ , making them suitable choices for partially shaded areas. Conversely, some plants thrive in high solar-irradiance conditions reaching up to  $3000 \text{ Wh/m}^2$ , including agave, lavender, rosemary, sunflowers, red pepper, tomatoes, peppers, basil, and others. The selection is compatible with Milan's weather and climatic conditions. Thus, these maps can also guide gardeners to choose crops suited to the irradiance, ensuring optimal growth and yield year-round.

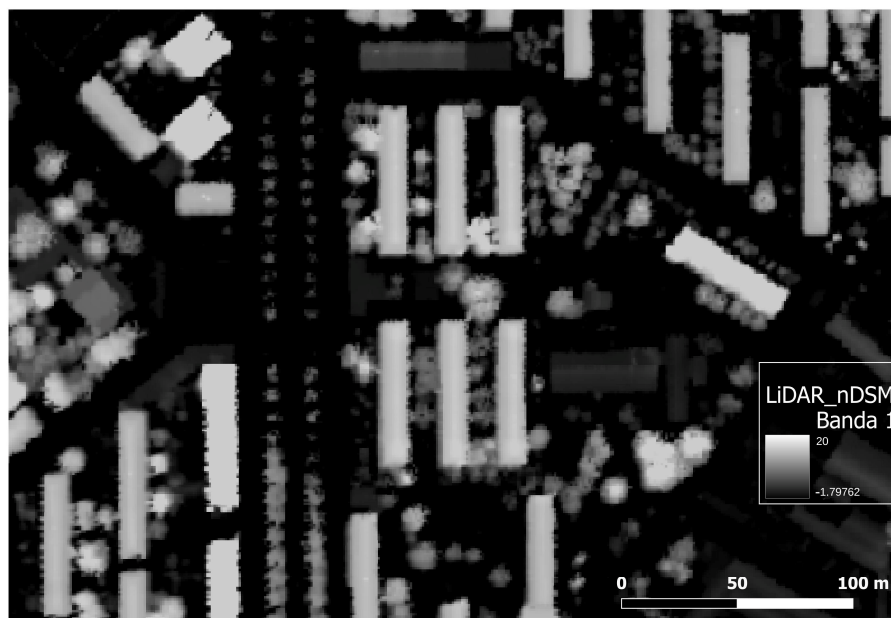


**Figure 3.** DEM developed from the LIDAR survey of the case study area. The legend illustrates the meters of height associated with the gray scale (source: Elaboration of the Authors).

#### 4.1.3. PAR and DLI Mapping

As mentioned before, PAR quantifies the solar radiation beneficial for plant production [19], while DLI represents the cumulative amount of PAR received by a surface throughout one day [20]. This metric is crucial for assessing the suitability of a location for plant growth based on the amount of light. Such a comparison could provide scientific support to the stakeholders to assess the adequacy of natural sunlight in different urban contexts (pertaining to crop placement, microclimate management, and seasonal planning) and how it aligns with the growing-light requirements of various crops. In the context of Italy, the National Agency for New Technologies (ENEA) has published maps detailing the average monthly DLI across the country, derived from data spanning from 2006 to 2020 [59]. These maps provide information on the climatic conditions conducive to agricultural food production in urban areas. For the same time frame, ENEA has published data on average daily global and diffuse solar radiation [59]. Comparing these data, measured in  $\text{Wh/m}^2$ , with the DLI, measured in  $\text{mol/m}^2\text{d}$ , reveals similar percentage reductions between the two metrics, differing by only 3%. For example, considering June and December as reference months, the global solar radiation in Milan showed values of  $6809 \text{ Wh/m}^2$  for June and  $1108 \text{ Wh/m}^2$  for December, indicating a 16% reduction between the two months. Correspondingly, the DLIs for June ranged between  $55 \text{ mol/m}^2\text{d}$  and  $60 \text{ mol/m}^2\text{d}$ , while for December, they were in the range of  $5\text{--}10 \text{ mol/m}^2\text{d}$ . The data published by ENEA [59] can be used to preliminarily assess the effectiveness of the conversion coefficients (Section 3.1.3). For example, consider a solar irradiation value of  $6809 \text{ Wh/m}^2$ . By multiplying this value by the estimated single conversion coefficient of  $0.00788688$ , we obtain a corresponding DLI of  $53.7 \text{ mol/m}^2/\text{day}$ . The calculated DLI value is slightly below the range specified by ENEA, which is between  $55$  and  $60 \text{ mol/m}^2/\text{day}$ . In December, the value for the average daily global solar irradiation on a horizontal plane amounted to  $1108 \text{ Wh}$ . By multiplying

this by the same conversion coefficient, we obtain an approximate DLI value for December of  $8.74 \text{ mol/m}^2/\text{d}$ , which falls within the range indicated by ENEA ( $5\text{--}10 \text{ mol/m}^2/\text{d}$ ). Based on the comparison with ENEA data, it is possible to state that the derived coefficient can be applied for an approximate estimation of the incident DLI variation from global horizontal irradiation maps generated using GIS. The map shown in Figure 4 presents the conversion of the values already presented in the GHI map, referring to a hypothetical plane at 4 m (Figure 5).

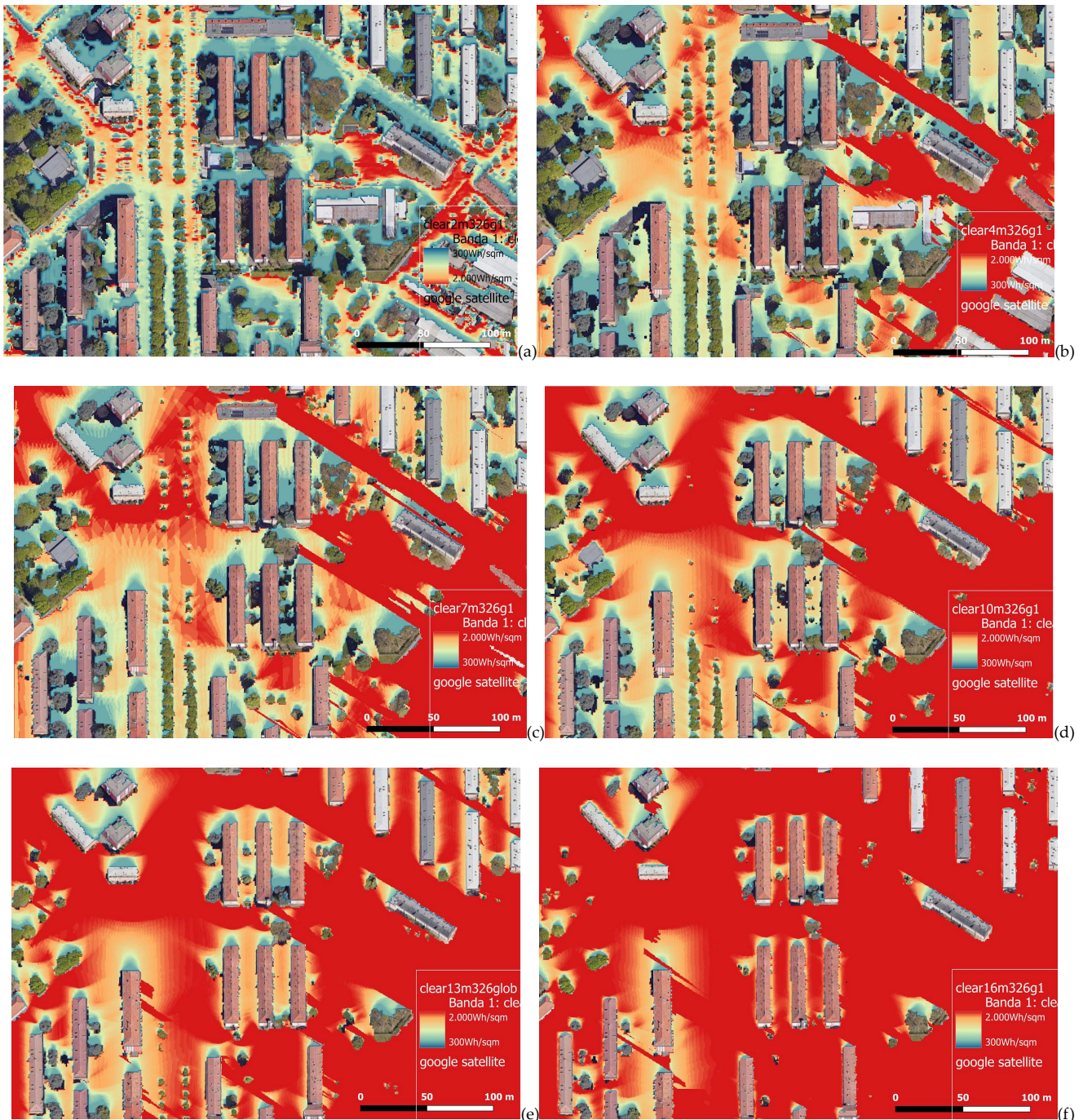


**Figure 4.** Map of global solar radiation on a fictitious horizontal plane relating to 21 November on a clear-sky day, unit of measurement  $\text{Wh/m}^2$ : (a) 2 m; (b) 4 m; (c) 7 m; (d) 10 m; (e) 13 m; (f) 16 m (source: Elaboration of the Authors).

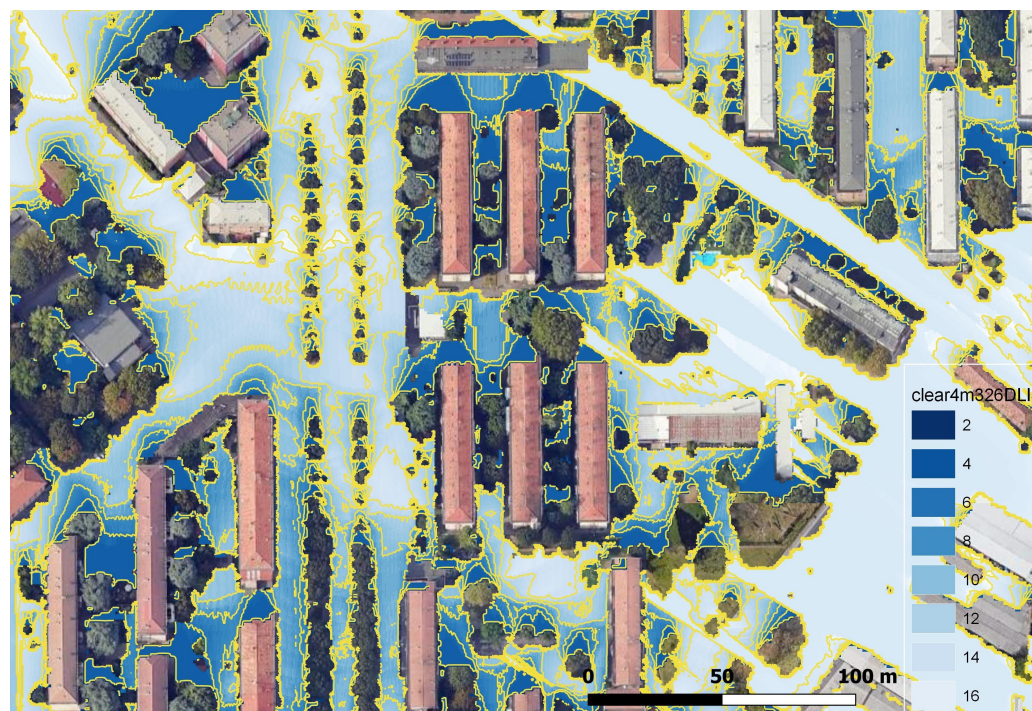


**Figure 5.** DLI map for 21 November under clear-sky conditions, measured in  $\text{mol}/\text{m}^2/\text{d}$  every two units (source: Elaboration of the Authors).

#### 4.1.4. Integration of the Digital Twin with Data Detected through Sensors

A significant contribution in terms of Digital Twin was developed through the integration of simulations of sensor data collected over 6 months period. A field survey was carried out. A pyranometer and a luxmeter were installed on a 6 m tall pole to collect data on natural lighting coming from the entire sky vault (Figure 6).



**Figure 6.** The sensor used in the survey: (a) The 6 m pole composed of the EKO pyranometer (center), the luxmeter (left), and the spectrometer (right, not evaluated in this study); (b) installation of the pole from the ground (source: Elaboration of the Authors).

The sensors are linked to a datalogger, which then transmits the gathered information to the telemetry site (Figure 7).

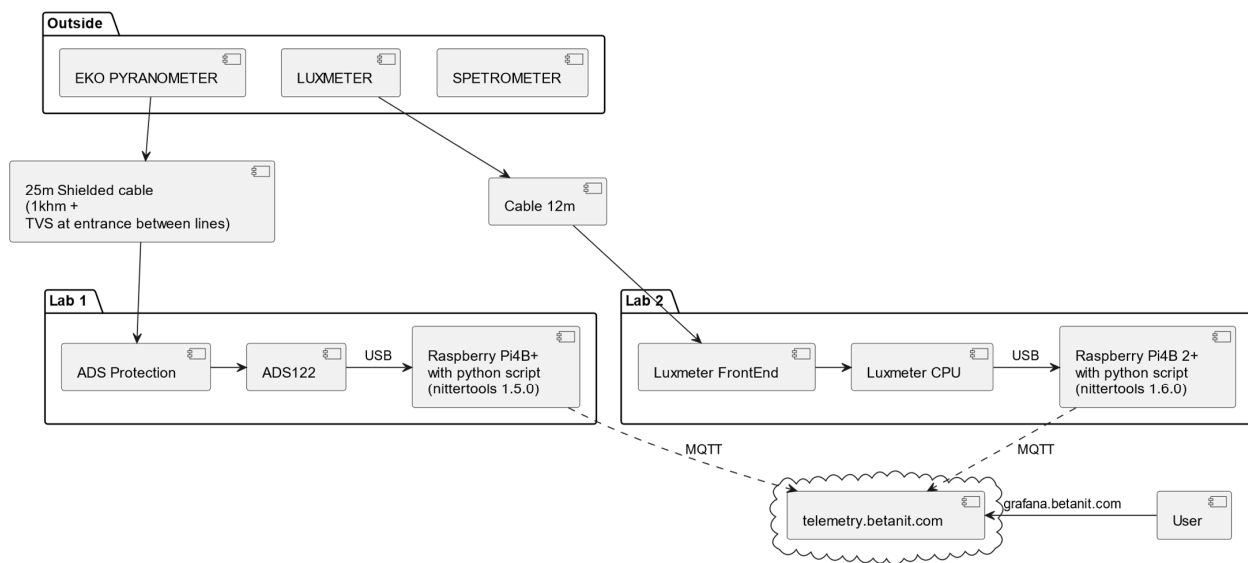


**Figure 7.** Overview of the key elements involved in the measurement system, including the pyranometer, luxmeter, spectrometer (not evaluated), datalogger, and telemetry site (source: Elaboration of the Authors).

The EKO pyranometer, model MS-402, is classified as a first-class device according to ISO9060 standards, boasting a rapid response time of less than 8 s. The output voltage from the pyranometer is converted to irradiance ( $\text{W}/\text{m}^2$ ) using two devices with comparable performance: an industrial-grade benchtop 6.5-digit digital multimeter (Keithley 2700) controlled with SCPI and a Betanit 24-bit ADC board. Approximately three readings per second are collected. Analysis of 1125 filtered measurements (Figure 8), extracted from 60 s data samples over three days in April 2024 (including two clear-sky days and one intermediate day: 13, 14, and 15), revealed a mean bias error of  $0.01 \text{ W}/\text{m}^2$  (after offset calibration), a mean bias error (MBS) percentage of 0.0001%, and a root mean square error (RMSE) percentage of 0.13% between the Keithley data and Betanit ADC data. The errors between the two systems are negligible; thus, the Betanit ADC was used as a cheaper and more compact alternative for the measurements. These readings were filtered to exclude obstructed views caused by nearby buildings and the sensors themselves.

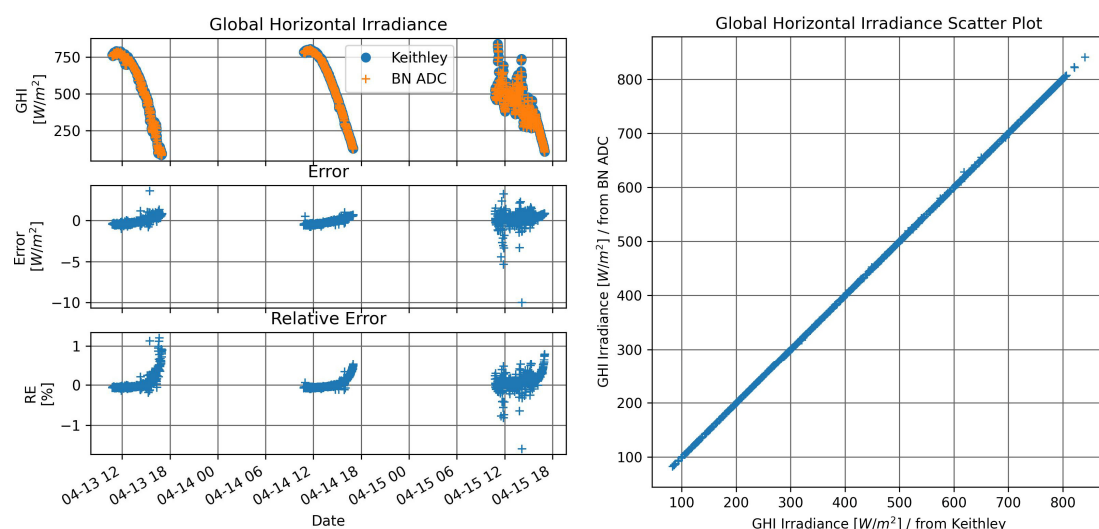


**Figure 8.** Comparison between the global horizontal irradiances recorded by the EKO pyranometer and converted by the Keithley DMM and those converted by the Betanit ADC (source: Elaboration of the Authors).



Both the Keithley 2700 digital multimeter and the Betanit 24-bit ADC board were managed using custom Python software 3.12. This software operates seamlessly on both Windows 11 and Raspberry Pi 4B platforms. The collected measurements were transmitted to the cloud telemetry site, hosted at <https://grafana.betanit.com> (Figure 9). This telemetry site utilizes two main technologies: InfluxDB for data persistence and Grafana for data visualization. The transmission of data to the telemetry site was facilitated via MQTT protocol, ensuring efficient and reliable data transfer.



**Figure 9.** Screenshot of the internal Grafana website for the initial exploration of raw data from the sensors. This example shows data collected on 12 April 2024. The upper chart displays the global horizontal irradiance measured with Keithley and Betanit; the middle chart shows the absolute error between the two measurements; and the bottom chart presents the relative error in percentage (Source: Elaboration of the Authors).

#### 4.2. Measurements and CAMS Estimations

After applying correction offsets for thermal effects (estimated at  $3 \text{ W/m}^2$ ) and datalogger offsets (estimated at  $0.71 \text{ W/m}^2$ ) [60], along with a correction factor (estimated through regression on sample sky data at 6.25%) due to obstructed sky views from nearby buildings and construction, the readings from the pyranometer were compared to the global horizontal irradiance published by CAMS for the same period. The readings from the pyranometer, after the application of correction offsets due to thermal (estimated  $3 \text{ W/m}^2$ ) and datalogger offset (estimated  $0.71 \text{ W/m}^2$ ) and a correction factor (estimated with regression on some sample sky to 6.25%) due to lacking a full view of the sky hemisphere due to nearby buildings and construction, was cross-checked to the global horizontal irradiance published by the CAMS solar radiation time series for the same time period (Figure 10).

For a timestep of 1 h between 27 November 2023 and 1 February 2024, with a limited window of 10 a.m. to 5 p.m., the mean bias error (MBE) was found to be  $4.6 \text{ W/m}^2$ , with a root mean square error (RMSE) of 26% based on approximately 475 observations. Reducing the timestep to 1 min resulted in greater errors in the CAMS data despite shortening the valid time window to 10 a.m. to 3 p.m. In this case, the MBE increased to  $27 \text{ W/m}^2$ , with an RMSE of 42% based on 20,769 individual measurements from the pyranometer (Figure 11).

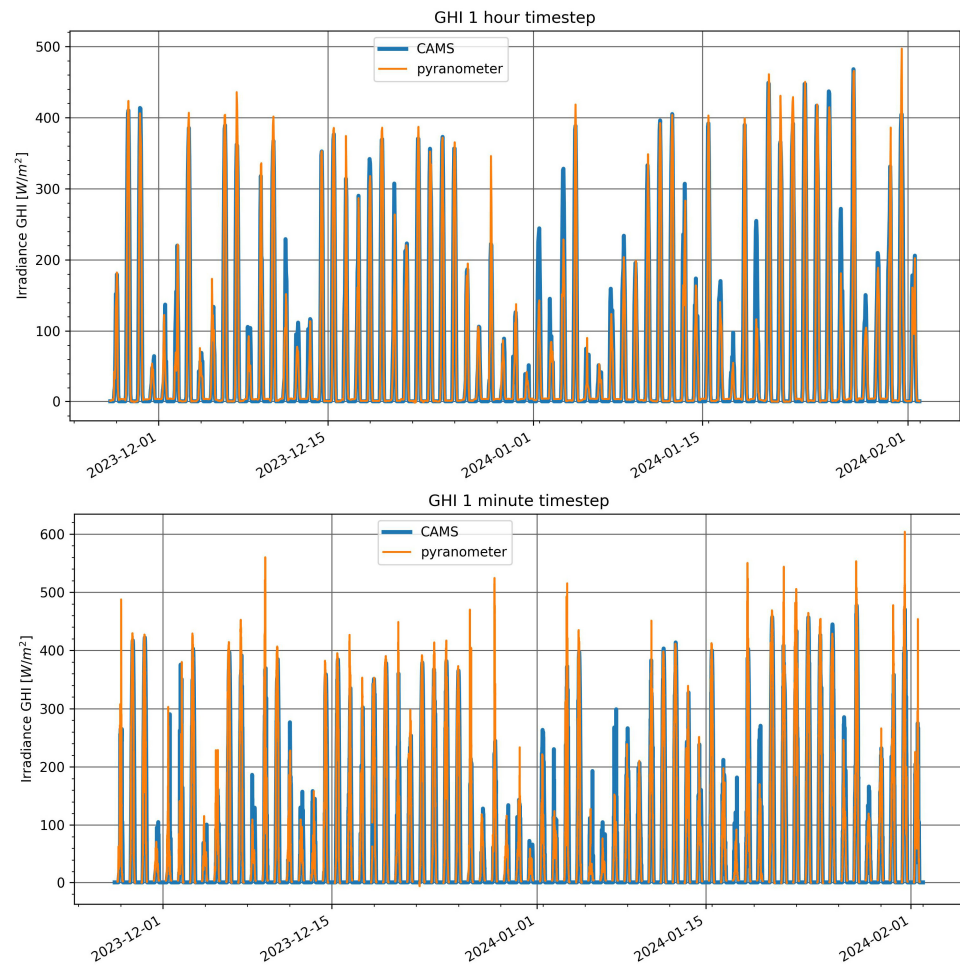


**Figure 10.** Graphics of the Global Horizontal Irradiances measured with the EKO pyranometer and Keithley or Betanit ADC (orange lines), alongside data provided by CAMS (blue lines, dataset: EO:ECMWF:DAT:CAMS\_SOLAR\_RADIATION\_TIMESERIES, with the *sky\_type* parameter set to “observed\_cloud”). The upper image represents a time step of 60 min, while the bottom image represents a time step of 1 min (source: Elaboration of the Authors).

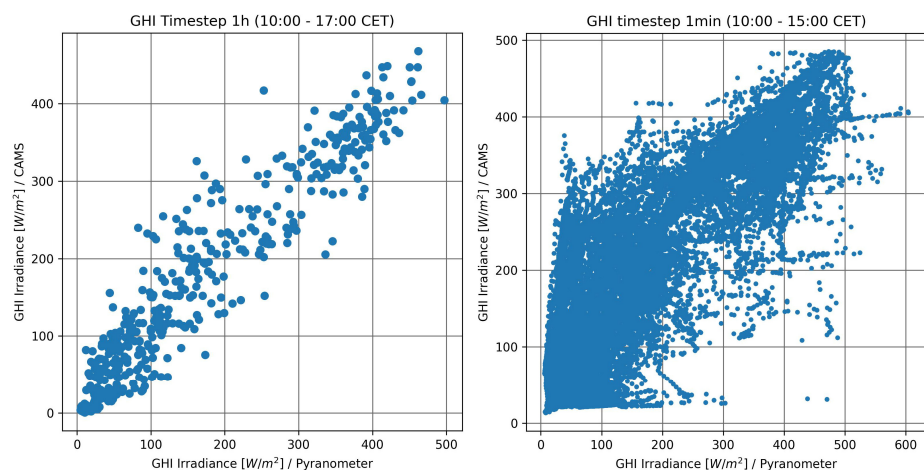


**Figure 11.** Comparison of the Global Horizontal Irradiances supplied by CAMS (dataset: EO:ECMWF:DAT:CAMS\_SOLAR\_RADIATION\_TIMESERIES, with the *sky\_type* parameter set to “observed\_cloud”) versus the data measured with the EKO pyranometer and Keithley or Betanit ADC. The left plot represents a time step of 60 min, while the right plot represents a time step of 1 min (source: Elaboration of the Authors).

These findings suggest that CAMS data provide a reasonable estimation when the simulation time base is not too short. At a 60 min timestep, CAMS data yielded an MBE of  $4.6 \text{ W/m}^2$  and an RMSE of 26%.

#### 4.3. Luminous Efficacy

Utilizing the irradiance (GHI) data collected by the pyranometer and the illuminances measured by the luxmeter (customized to waterproof their luxmeter model nut) positioned adjacent to the pyranometer, we assessed the luminous efficacy of global radiation for a select number of days from 24 April to 14 May, with a timestep of 1 min. Following the removal of out-of-bounds measurements and those influenced by shadows from nearby objects and sensors, we identified approximately 7062 samples obtained during midday hours (from 10:30 to 17:00 local time). Our analysis revealed that the highest frequency of luminous efficacy fell within the 100–110  $\text{lm/W}$  range, confirming the suitability of the Italian model. Conversely, the lowest frequency, observed in the 70–80  $\text{lm/W}$  range, coincided with periods of rainfall (Figure 12).

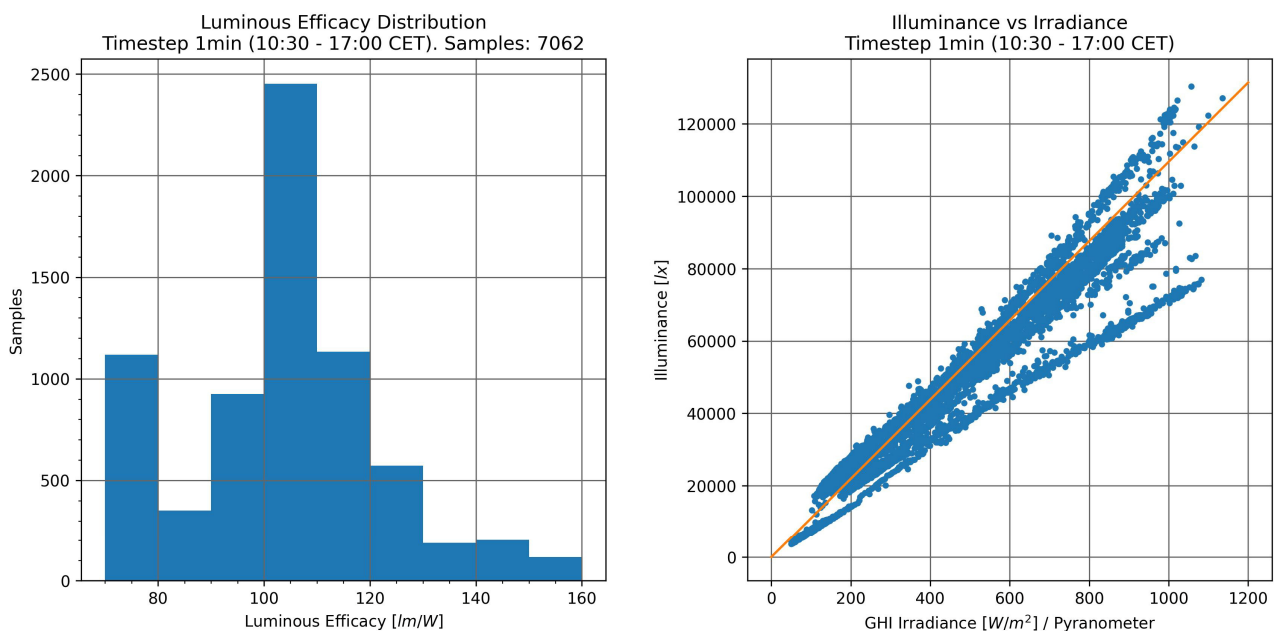


**Figure 12.** On the left: the distribution of the luminous efficacy in bins of 10  $\text{lm/W}$ . On the right: the comparison between Global Horizontal Irradiance and the measured illuminance, with the orange line representing the Cucumo et al. [52] efficacy model (source: Elaboration of the Authors).

The constant value proposed by Cucumo et al. [52] is proposed as a preliminary approach for the conversion of the GHI provided by CAMS irradiances into illuminances. Nevertheless, further evaluations concerning the spectrum of radiation and its effectiveness in plant growth are essential to ensure the accuracy of subsequent analyses.

This correlation facilitates a more practical and straightforward examination of the relationships between solar irradiation (including GHI, BHI, DHI, and BNI) and the illuminance values of natural sunlight (involving both incident and diffuse light). November in Italy typically marks the transition from fall to winter, characterized by shorter days and lower angles of sunlight. Conversely, April marks the transition from winter to spring, characterized by longer days and higher angles of sunlight. The selection of these temporal intervals permits a comprehensive examination of the seasonal variations in solar radiation and their consequent impact on natural lighting levels. The consistency of measurements allows for the precise documentation of these fluctuations, thereby enhancing the understanding of the influence of solar radiation on perceived luminance levels, particularly in urban environments characterized by diverse contextual factors such as vegetation, nearby

structures, and geographical positioning. The data collected during this working phase provide a foundation for future research developments. In particular, the recording of fluctuations in values associated with luminous efficacy would permit the definition of more accurate dynamic conversion coefficients, which could be published on an hourly basis based on the recorded data.

At the current stage of the method application phase, the measurements made with sensors confirm the feasibility of using solar radiation data published in CAMS database to develop solar maps reflecting actual radiation conditions at an interval of 60 min (as part of the digital twin model). The survey activity also confirmed the reliability of the conversion coefficients from solar radiation to natural lighting adopted in the methodology and proposed by Cucumo [52]. What has been illustrated so far allows for the development of maps at different heights, incorporating various units of measurement related to the quantity of incident energy, natural lighting, and DLI.

Future developments concern the possibility of combining the mapped data with a database of possible solutions that can be adopted based on the actual quantities of available energy and lighting. This information will concern the different plants that can be cultivated in the climates of Milan and Singapore as well as various envelope solutions that optimize the use of solar radiation conditions to reduce the energy needs of buildings. As regards this last point, it refers to energy for cooling internal spaces in both contexts and energy for winter heating for the Italian context only. Regarding the limits associated with the application phase, it is important to point out that the available LIDAR surveys are not updated annually, which may result in changes in the obstructions related to vegetation over time. Furthermore, with reference to the same topic, at the moment, the LIDAR maps do not allow to identify the type of plant and therefore to assess the seasonal variations in obstruction due to the possible loss of leaves in the winter period. In this regard, possible further elaborations could concern the overlay of point maps of the trees that include information on the species being developed by the municipality of Milan and the LIDAR maps. Such processing would allow identifying the portions of the LIDAR affected by deciduous plants.

## 5. Conclusions

This study introduces the methodology and application of an open-source GIS-based Digital Twin model designed for solar radiation mapping to support sustainable urban agriculture design. The development of this Digital Twin model aims to facilitate the integration of urban agriculture systems into building environments. The analysis highlights that the current availability of open data and open-source software can be valorized and used to scrutinize specific situations through field surveys and demonstrates that the seamless integration between data and computational procedures is possible. For example, the maps reported in Figures 4 and 5 were developed based on the combination of open data and conversion factors, which are measured data and could be further expanded and tested in different geographical and climatic conditions. As reported in Section 4.1.3, a reliable simulation could be obtained for at least a 60 min timestep. According to this, the methodology presented in the paper would allow the realization of maps based on hourly data, which means that a more sophisticated analysis is possible, which would be helpful for better understanding the potential of green building integration.

Very often, data related to plant productivity, like light requirements, are not easily legible for everybody [61]. The use of maps, a tool that combines different information, could help different users and urban farmers (usually not expert farmers) to better understand how to enhance the potential of the area.

This capability proves essential for generating irradiance maps that accurately reflect real-world conditions, thereby identifying variations in solar energy quantities on horizontal surfaces within the urban fabric. The Digital Twin model significantly enhances the precision of solar radiation mapping, essential for optimizing crop productivity in urban settings. The following key findings can be highlighted:

- Mapping solar irradiance levels facilitates the optimization of resources such as energy and water in urban agriculture (e.g., with precise insight into available sunlight levels, irrigation and artificial lighting can be adjusted to maximize plant growth and enhance crop yields). At the urban level, the availability of precise information about the different potentials of the areas used for urban farming allows us to calculate the environmental impact of the urban farm; for instance, what is the potential of absorption of CO<sub>2</sub> and other gases for limiting the greenhouse effect, improving the air quality, or reducing the overheating? Our way of thinking about green infrastructure would change: The point would not be linked to greening the available areas but trying to involve all the surfaces with high potential, namely facades at specific orientations and at specific levels with suitable characteristics, as pieces of a puzzle for which we can acquire a sense if we see the city in its 3D shape;
- Understanding solar irradiance distribution and equity in urban areas empowers urban planners' residents and public administrators to identify the most suitable locations for urban agriculture initiatives. In this field, a better cooperation between agronomists (as experts in plants requirements) and urban planners/architects could be beneficial, and in case of urban renewal programs or building upgrading, a public–private partnership could affect some decisions aimed at improving farming production. As part of this process, residents could be involved and made aware about the potential of their home. In the case of the communal areas such as rooftops or lots, especially when the solar radiation reaches the surface differently, the urban farmers could be informed about the different potential of the specific areas (for instance, the number of hours of sun exposure compatible with specific groups of plants);
- Knowledge of solar-irradiance levels can inform the formulation of tailored policies to support urban agriculture, such as tax incentives for using sustainable technologies or regulations for the protection of designated agricultural areas. The incentives could be considered to encourage people, especially owners of more suitable surfaces, to convert them into farming areas. For public infrastructures, i.e., schools, libraries, gyms, etc., a list of the suitable areas could be produced and people involved, especially in the case of the promotion of local food or food security.

**Author Contributions:** Conceptualization, M.C. and V.D.; methodology, M.C. and E.L.; validation, G.M.P. and S.-C.C.; formal analysis, M.C. and E.L.; investigation, M.C., G.M.P. and E.L.; software, M.C. and G.M.P.; writing—original draft preparation, E.L., G.M.P. and M.C.; writing—review and editing, M.C., V.D., G.M.P., S.-C.C., B.A.T.W. and E.L.; project administration, E.L., V.D. and S.-C.C.; supervision, M.C., V.D. and E.L.; funding acquisition, V.D. and S.-C.C. All authors have read and agreed to the published version of the manuscript.

**Funding:** The paper reports parts of the research “*Bize\_UrFarm: Building Integrated Zero Emission Urban Farming towards sustainable farmscape in Milan and Singapore*”, funded jointly by the Italian Ministry of Foreign Affairs and International Cooperation (MAECI) Project n. SG23GR02 and Singapore Agency for Science, Technology and Research (A\*STAR) First Executive Programme of Scientific and Technological Cooperation (Italy–Singapore), project No. R23I0IR035.

**Informed Consent Statement:** Not applicable.

**Data Availability Statement:** The original contributions presented in the study are included in the article, further inquiries can be directed to the corresponding author.

**Conflicts of Interest:** Author Giulio Maria Podestà was employed by the company Nitter Betanit. The remaining authors declare that the research was conducted in the absence of any commercial or financial relationships that could be construed as a potential conflict of interest.

## References

1. Yuan, G.N.; Marquez, G.P.B.; Deng, H.; Iu, A.; Fabella, M.; Salonga, R.B.; Ashardiono, F.; Cartagena, J.A. A review on urban agriculture: Technology, socio-economy, and policy. *Heliyon* **2022**, *8*, e11583. [[CrossRef](#)]

2. Smit, J.; Ratta, A.; Nasr, J. Urban Agriculture: Food, Jobs and Sustainable Cities, The Urban Agriculture Network, United Nations Development Programme (1996). Available online: <https://urban.agroeco.org/wp-content/uploads/2015/12/UNDP-Urban-Agriculture-Part-one-1.pdf> (accessed on 26 May 2024).
3. Orsini, F.; Kahane, R.; Nono-Womdim, R.; Gianquinto, G. Urban agriculture in the developing world: A review. *Agron. Sustain. Dev.* **2013**, *33*, 695–720. [[CrossRef](#)]
4. Artmann, M.; Sartison, K. The role of urban agriculture as a nature-based solution: A review for developing a systemic assessment framework. *Sustainability* **2018**, *10*, 1937. [[CrossRef](#)]
5. Nicholls, E.; Ely, A.; Birkin, L.; Basu, P.; Goulson, D. The contribution of small-scale food production in urban areas to the sustainable development goals: A review and case study. *Sustain. Sci.* **2020**, *15*, 1585–1599. [[CrossRef](#)]
6. Al-Kodmany, K. The vertical farm: A review of developments and implications for the vertical city. *Buildings* **2018**, *8*, 24. [[CrossRef](#)]
7. Appolloni, E.; Orsini, F.; Specht, K.; Thomaier, S.; Sanye-Mengual, E.; Pennisi, G.; Gianquinto, G. The global rise of urban rooftop agriculture: A review of worldwide cases. *J. Clean. Prod.* **2021**, *296*, 126556. [[CrossRef](#)]
8. Aptekar, S. Visions of public space: Reproducing and resisting social hierarchies in a community garden. *Sociol. Forum* **2015**, *30*, 209–227. [[CrossRef](#)]
9. Aubry, C.; Manouchehri, M. Urban agriculture and health: Assessing risks and overseeing practices. *Field Actions Sci. Rep.* **2019**, *20*, 108–111.
10. Dubbeling, M.; Veenhuizen, R.; Halliday, J. Urban agriculture as a climate change and disaster risk reduction strategy. *Field Actions Sci. Rep.* **2019**, *20*, 32–39.
11. Azunre, G.A.; Amponsah, O.; Peprah, C.; Takyi, S.A.; Braimah, I. A review of the role of urban agriculture in the sustainable city discourse. *Cities* **2019**, *93*, 104–119. [[CrossRef](#)]
12. Pluchino, P. *La Città Vivente. Introduzione al Metabolismo Urbano Circolare*; Malcor D' ed.: Catania, Italy, 2019.
13. Wolman, A. The metabolism of cities. *Sci. Am.* **1965**, *213*, 179–190. [[CrossRef](#)]
14. Tang, M.; Hong, J.; Guo, S.; Liu, G.; Shen, G.Q. A bibliometric review of urban energy metabolism: Evolutionary trends and the application of network analytical methods. *J. Clean. Prod.* **2021**, *279*, 123403. [[CrossRef](#)]
15. Smith, R.; Houtman, J.; Stwalley, R.M. Send mail to Stwalley R.M., IIIA site suitability approach to sustainable urban agriculture using GIS and decision analysis. In Proceedings of the 2017 ASABE Annual International Meeting, Spokane, DC, USA, 16–19 July 2017.
16. Dessì, V.; Clementi, M. Mapping Urban Water Balance to support the integrated design of water cycles in the peri-urban areas. *J. Phys. Conf. Ser.* **2023**, *2600*, 172005. [[CrossRef](#)]
17. Abdulkadir, A.; Leffelaar, P.A.; Agbenin, J.O.; Giller, K.E. Nutrient flows and balances in urban and peri-urban agroecosystems of Kano, Nigeria. *Nutr. Cycl. Agroecosyst.* **2013**, *95*, 231–254. [[CrossRef](#)]
18. Yuan, C.; Chen, L. Mitigating urban heat island effects in high-density cities based on sky view factor and urban morphological understanding: A study of Hong Kong. *Archit. Sci. Rev.* **2011**, *54*, 305–315. [[CrossRef](#)]
19. JDu, S. Sharples, Biophilic Atrium Design: An Analysis of Photosynthetically Active Radiation for Indoor Plant Systems: Comparison between Two Climates. In Proceedings of the PLEA 2020—35th PLEA Conference on Passive and Low Energy Architecture Planning Post Carbon Cities, Proceedings, A Coruna, Spain, 1–3 September 2020.
20. Tan, P.Y.; Ismail, M.R. Photosynthetically active radiation and comparison of methods for its estimation in equatorial Singapore. *Theor. Appl. Climatol.* **2016**, *123*, 873–8831. [[CrossRef](#)]
21. Udo, S.O.; Aro, T.O. Global PAR related to global solar radiation for central Nigeria. *Agric. For. Meteorol.* **1999**, *97*, 21–31. [[CrossRef](#)]
22. Marchwiński, J.; Milošević, V.; Stefańska, A.; Lucchi, E. Irradiation Analysis of Tensile Membrane Structures for Building-Integrated Photovoltaics. *Energies* **2023**, *16*, 5945. [[CrossRef](#)]
23. Lucchi, E.; Adami, J.; Peluchetti, A.; Mahecha Zambrano, J.C. Photovoltaic potential estimation of natural and architectural sensitive land areas to balance heritage protection and energy production. *Energy Build.* **2023**, *290*, 113107. [[CrossRef](#)]
24. Pradhan, P. A systematic review highlights that there are multiple benefits of urban agriculture besides food. *Glob. Food Secur.* **2023**, *38*, 100700. [[CrossRef](#)]
25. Benedetti, A.C.; Costantino, C.; Gulli, R.; Predari, G. The Process of Digitalization of the Urban Environment for the Development of Sustainable and Circular Cities: A Case Study of Bologna (Italy). *Sustainability* **2022**, *14*, 13740. [[CrossRef](#)]
26. Lucchi, E. Digital twins for the automation of the heritage construction sector. *Autom. Constr.* **2023**, *156*, 105073. [[CrossRef](#)]
27. Naval, A.; Kumar, V.; Gaurav, K. Quantifying Vertical Farming Potential Using Digital Twins. *Lect. Notes Netw. Syst. (LNNS)* **2023**, *765*, 427–436.
28. Ghandar, A.; Ahmed, A.; Zulfikar, S.; Hanai, M.; Theodoropoulos, G. A Decision Support System for Urban Agriculture Using Digital Twin: A Case Study With Aquaponics. *IEEE Access* **2021**, *9*, 35691–35708. [[CrossRef](#)]
29. Mengi, E.; Becker, C.J.; Sedky, M.; Yu, S.-Y.; Zohdi, T.I. A Digital-Twin and Rapid Optimization Framework for Optical Design of Indoor Farming Systems. *Comput. Mech.* **2024**, *74*, 31–43. [[CrossRef](#)]

30. Gabriele, M.; Cazzani, A.; Zerbi, C.M.; Brumana, R. Digital Twin to Monitor, Understand and Preserve the Complexity of Multi-Scale Natural, Agricultural, Designed Landscapes and Architecture: Biodiversity Conservation, Transformation and Decline at Villa Arconati Site at Castellazzo of Bollate (MI). *Int. Arch. Photogramm. Remote Sens. Spat. Inf. Sci. ISPRS Arch.* **2023**, *48*, 613–620. [CrossRef]
31. Shahzad, M.; Shafiq, M.T.; Douglas, D.; Kassem, M. Digital, Twins in Built Environments: An Investigation of the Characteristics, Applications, and Challenges. *Buildings* **2022**, *12*, 120. [CrossRef]
32. QGIS Software. Available online: <https://qgis.org/it/site> (accessed on 26 May 2004).
33. GRASSGIS Website. Available online: <https://grass.osgeo.org> (accessed on 26 May 2024).
34. gvSIG Website. Available online: <http://www.gvsig.com> (accessed on 26 May 2024).
35. Hofierka, J.; Suri, M. The solar radiation model for open-source GIS: Implementation and applications. In Proceedings of the Open-Source GIS-GRASS Users Conference, Trento, Italy, 11–13 September 2002; Ciolli, M., Zatelli, P., Eds.; University of Trento: Trento, Italy, 2002.
36. Meteorological Stations Data. Available online: <https://www.dati.lombardia.it/Ambiente/stazioni-meteo/pevf-9zqp> (accessed on 3 March 2024).
37. Photovoltaic Geographical Information System. Available online: [https://re.jrc.ec.europa.eu/pvg\\_tools/en](https://re.jrc.ec.europa.eu/pvg_tools/en) (accessed on 20 March 2024).
38. Chatzipoulka, C.; Compagnon, R.; Nikolopoulou, M. Urban geometry and solar availability on façades and ground of real urban forms: Using London as a case study. *Sol. Energy* **2016**, *138*, 53–66. [CrossRef]
39. Mosharafian, S.; Afzali, S.; Weaver, G.M.; van Iersel, M.; Velni, J.M. Optimal lighting control in greenhouse by incorporating sunlight prediction. *Comput. Electron. Agric.* **2020**, *188*, 106300. [CrossRef]
40. Terashima, I.; Fujita, T.; Inoue, T.; Chow, W.S.; Oguchi, R. Green Light Drives Leaf Photosynthesis More Efficiently than Red Light in Strong White Light: Revisiting the Enigmatic Question of Why Leaves are Green. *Plant Cell Physiol.* **2009**, *50*, 684–697. [CrossRef]
41. Hall, D.O.; Rao, K. *Photosynthesis*; Cambridge University Press: Cambridge, UK, 1999.
42. Ocampo, A.L. Development of Data Acquisition Model for Daily Light Integral Measurement. 27 December 2017. Available online: <https://po.pnuresearchportal.org/ejournal/index.php/apherj/article/view/559> (accessed on 1 July 2024).
43. Lee, S.; Park, S. Energy savings of home growing plants by using daylight and LED. In Proceedings of the 2013 IEEE Sensors Applications Symposium Proceedings, Galveston, TX, USA, 19–21 February 2013.
44. Jarzyna, K.; Podgorska, M.; Szwed, M.; Jozwiak, M. A Simple Light Meter as a Device for Studying the Influence of Seasonal Changes of Light Conditions on the Phenology of Herbaceous Under-Growth Species in a Fertile Beach. Forest. 2018. Available online: [https://www.academia.edu/download/60331969/Baltic\\_Forestry\\_2018.1\\_148-15720190819-113009-esacox.pdf](https://www.academia.edu/download/60331969/Baltic_Forestry_2018.1_148-15720190819-113009-esacox.pdf) (accessed on 26 May 2024).
45. Mazzelli, A.; Cicci, A.; Caprio, F.D.; Altimari, P.; Toro, L.; Iaquaniello, G.; Pagnanelli, F. Multivariate Modeling for Microalgae Growth in Outdoor Photobioreactors. *Algal Res.* **2020**, *45*, 101663. [CrossRef]
46. Ashdown, I. Photometry and Photosynthesis. 10 December 2014. Available online: <https://www.allthingslighting.org/tag/lighting-fundamentals/> (accessed on 26 May 2024).
47. Fang, D.; Arsano, A.; Brown, N.; Reinhart, C.; Mueller, C. Design Space Exploration for High-Performance Greenhouse Design. 7 October 2019. Available online: <https://www.ingentaconnect.com/content/iass/piass/2019/00002019/00000016/art00006> (accessed on 26 May 2024).
48. Alahakoon, P.K. Productivity, Photosynthesis and Nitrogen Metabolism of Various Leafy Vegetables Grown Aeroponically under Different Combinations of Light-Emitting Diodes (LEDs). 2016. Available online: <https://repository.nie.edu.sg/handle/10497/22434> (accessed on 26 May 2024).
49. Torres, A.P.; Lopez, R.G. Measuring Daily Light Integral in a Greenhouse. 2010. Available online: <https://www.extension.purdue.edu/extmedia/ho/ho-238-w.pdf> (accessed on 26 May 2024).
50. Mattson, N. Greenhouse Lighting. Available online: <https://courses.cit.cornell.edu/hort494/greenhouse/lighting/lightlft.html> (accessed on 26 May 2024).
51. Song, X.P.; Tan, H.T.; Tan, P.Y. Assessment of Light Adequacy for Vertical Farming in a Tropical City. *Urban For. Urban Green.* **2018**, *29*, 49–57. [CrossRef]
52. Cucumo, M.A.; De Rosa, A.; Ferrero, V.; Kaliakatsos, D.; Marinelli, V. Correlazioni sperimentali dell'efficacia luminosa della radiazione globale, diretta e diffusa. In Proceedings of the 59° Congresso ATI, Genova, Italy, 14–17 September 2004.
53. TMY Calculator in the Photovoltaic Geographical Information System. Available online: [https://re.jrc.ec.europa.eu/pvg\\_tools/en/#TMY](https://re.jrc.ec.europa.eu/pvg_tools/en/#TMY) (accessed on 26 May 2024).
54. CAMS Solar Radiation Time Series. Available online: <https://ads.atmosphere.copernicus.eu/cdsapp#!/dataset/cams-solar-radiation-timeseries?tab=overview> (accessed on 26 May 2024).
55. Littlefair, P.J. The luminous efficacy of daylight: A review. *Light. Res. Technol.* **1985**, *17*, 162–182. [CrossRef]
56. ISTAT: Basi Territoriali e Variabili Censuarie, Censimento Della Popolazione e Delle Abitazioni 2011 (2012). Available online: <https://www.istat.it/it/archivio/104317> (accessed on 26 May 2024).

57. Morganti, M.; Clementi, M.; Rogora, A. Open-Source Integrated Mapping of Urban Form and Solar Radiation for Environmental Design. In *Sustainability in Energy and Buildings 2021*; Littlewood, J.R., Howlett, R.J., Lakhmi, C.J., Eds.; Springer: Berlin/Heidelberg, Germany, 2022; pp. 377–386.
58. Google Maps. Available online: <https://www.google.it/maps> (accessed on 26 May 2024).
59. Enea: Italian Solar Radiation Atlas. Available online: <http://www.solaritaly.enea.it/DLI/DLIMappeEn.php> (accessed on 26 May 2024).
60. Sanchez, G.; Serrano, A.; Cancillo, M.L.; Garcia, J.A. Pyranometer Thermal Offset: Measurement and Analysis. *J. Atmos. Oceanic Technol.* **2015**, *32*, 234–246. [[CrossRef](#)]
61. Morulanda, C.; Izquierdo, J. *Popular Hydroponic Gardens. Technical Manual*; FAO and UNDP, FAO Regional Office for Latin America and the Caribbean: Santiago del Chile, Chile, 1993.

**Disclaimer/Publisher’s Note:** The statements, opinions and data contained in all publications are solely those of the individual author(s) and contributor(s) and not of MDPI and/or the editor(s). MDPI and/or the editor(s) disclaim responsibility for any injury to people or property resulting from any ideas, methods, instructions or products referred to in the content.